Employing PEDOT as the p–Type Charge Collection Layer in Regular Organic–Inorganic Perovskite Solar Cells

ARTICLE *in* JOURNAL OF PHYSICAL CHEMISTRY LETTERS · APRIL 2015

Impact Factor: 7.46 · DOI: 10.1021/acs.jpclett.5b00545

8 AUTHORS, INCLUDING:

Thomas Stergiopoulos
Aristotle University of Thessaloniki
69 PUBLICATIONS **2,486** CITATIONS
SEE PROFILE

Tomas Leijtens
Stanford University
29 PUBLICATIONS **2,336** CITATIONS
SEE PROFILE

Konrad Wojciechowski
University of Oxford
15 PUBLICATIONS **682** CITATIONS
SEE PROFILE

Stefan Schumann
Heraeus Holding
19 PUBLICATIONS **268** CITATIONS
SEE PROFILE

THE JOURNAL OF PHYSICAL CHEMISTRY Letters

Letter

pubs.acs.org/JPCL

Employing PEDOT as the p-Type Charge Collection Layer in Regular Organic–Inorganic Perovskite Solar Cells

Jiewei Liu,[†] Sandeep Pathak,[†] Thomas Stergiopoulos,[†] Tomas Leijtens,[†] Konrad Wojciechowski,[†] Stefan Schumann,[‡] Nina Kausch-Busies,[‡] and Henry J. Snaith*[,†]

[†]Clarendon Laboratory, Department of Physics, University of Oxford, Parks Road, Oxford, OX1 3PU, United Kingdom

[‡]Heraeus Deutschland GmbH & Co. KG, Business Line Display and Semiconductors (HNB), Chempark Leverkusen / Gebäude B 202, D-51368 Leverkusen, Germany

Supporting Information

ABSTRACT: Organic–inorganic halide perovskite solar cells have recently emerged as high-performance photovoltaic devices with low cost, promising for affordable large-scale energy production, with laboratory cells already exceeding 20% power conversion efficiency (PCE). To date, a relatively expensive organic hole-conducting molecule with low conductivity, namely spiro-OMeTAD (2,2′,7,7′-tetrakis(*N*,*N*-di-*p*-methoxyphenyl-amine) 9,9′- spirobifluorene), is employed widely to achieve highly efficient perovskite solar cells. Here, we report that by replacing spiro-OMeTAD with much cheaper and highly conductive poly(3,4-ethylenedioxythiophene) (PEDOT) we can achieve PCE of up to 14.5%, with PEDOT cast from a toluene based ink. However, the stabilized power output of the PEDOT-based devices is only 6.6%, in comparison to 9.4% for the spiro-OMeTAD-based cells. We deduce that accelerated recombination is the cause for this lower stabilized power output and postulate that reduced levels of p-doping are required to match the stabilized performance of Spiro-OMeTAD. The entirely of the materials employed in the perovskite solar cell are now available at commodity scale and extremely inexpensive.

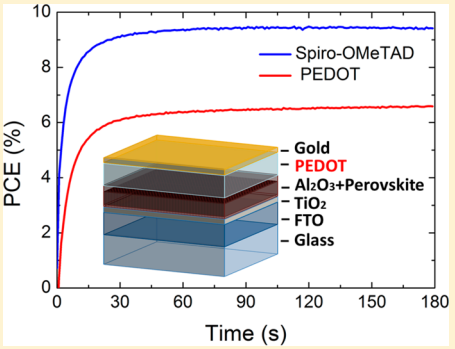

The application of photovoltaic (PV) devices is one of the most promising solutions for satisfying the global energy demand.[1] Recently, organic–inorganic metal halide perovskite ($CH_3NH_3PbX_3$ (X = I^-, Br^-, Cl^-)) has emerged as a promising photovoltaic material, with simple fabrication routes and high power conversion efficiency, with small area lab cells certified up to ∼20.1%.[2] These perovskites were first employed in liquid dye solar cells employing iodide/triiodide redox couples, but this only delivered 3.5% efficient cells and degraded within a few minutes.[3] The first big breakthrough in device architecture was in-part a result of employing the organic hole-conductor 2,2′,7,7′-tetrakis(*N*,*N*-di-*p*-methoxyphenyl-amine) 9,9′- spirobifluorene (spiro-OMeTAD), delivering solar cell efficiencies of around 10%.[4,5] However, the spiro-OMeTAD has a price at research scale that is more than 10 times that of gold and platinum.[6] It is likely that this would come down considerably with increasing scale. However, the multistep synthesis and time-consuming purification (sublimation) imply that it would be a significant component of the cost of the first commercial products for some time. There is therefore good motivation to develop perovskite cells based on already scaled "commodity" hole-conductors such as CuSCN,[7] CuI,[6] polyaniline, or poly(3,4-ethylenedioxythiophene) (PEDOT) among others. PEDOT specifically is an inexpensive conducting polymer with high conductivity and has long been applied in both organic photovoltaics and light emitting diodes as a charge collection or charge injection layer.[8−11] However, PEDOT is typically heavily doped by being stabilized with polystyrenesulfonate (PSS) and processed into an aqueous dispersion. Since the organic–inorganic metal halide perovskites are sensitive to moisture, this makes processing of PEDOT:PSS directly on top of the perovskite film challenging. Hence, although there are many reports of PEDOT:PSS employed in a device structure where the perovskite is processed on top of the cathode (and PEDOT:PSS layer on top of FTO or ITO transparent conductive glass),[12] there are no reports yet that we are aware of where PEDOT is processed on top of the perovskite in a "regular" device architecture. Here, we employ a specifically formulated PEDOT ink (Clevios NKB 717, Heraeus Deutschland GmbH & Co. KG), which is a dispersion of poly(3,4-ethylenedioxythiophene) and a sulfonated block-*co*-polymer dispersed in toluene, as a hole-transporting material (HTM). We achieve comparable power conversion efficiency to spiro-OMeTAD based cells, of up to 14.5%, employing this much lower cost hole-transporter. However, the steady-state stabilized power output is much lower for the PEDOT cells than for the spiro-OMeTAD cells. We investigate the origin of this reduced stabilized power output and identify future development directions for enhancing the perovskite solar cells employing PEDOT.

Received: March 14, 2015
Accepted: April 13, 2015

DOI: 10.1021/acs.jpclett.5b00545
J. Phys. Chem. Lett. 2015, 6, 1666−1673

To determine the suitability of PEDOT as an HTM processed on top of the perovskite layer in hybrid perovskite solar cells, we first investigated the optical and photophysical properties of spiro-OMeTAD and PEDOT films isolated and in contact with perovskite films. We show the UV−vis absorption of the two HTMs in Figure 1a. The spectra match those

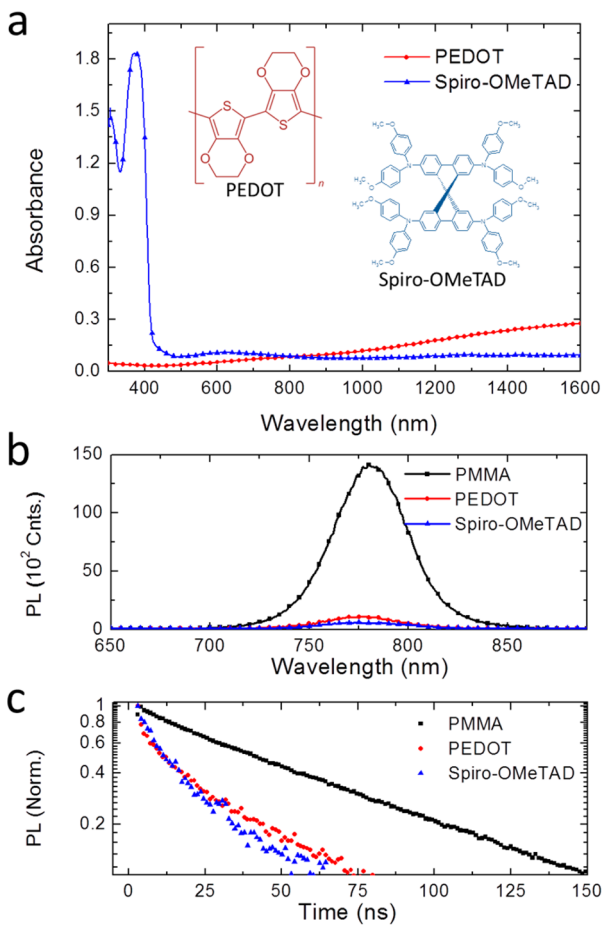

Figure 1. (a) Absorbance spectra of ∼230 nm thick PEDOT films (red circles) and ∼280 nm thick spiro-OMeTAD films doped with Li-TFSI and (blue triangles) deposited on glass. (b) Steady-state PL spectra and (c) time-resolved PL decay exited at 507 nm of perovskite films coated with PMMA (black squares), PEDOT (red circles), and Spiro-OMeTAD (blue triangles), respectively.

previously reported for the two materials.[8,13] Spiro-OMeTAD films exhibit a strong absorption in ultraviolet region (<400 nm), along with weaker absorption bands at 500 and 670 nm associated with the oxidized spiro-OMeTAD species. By contrast, the absorbance of PEDOT films is very low in the UV and visible region, while slightly higher than that of spiro-OMeTAD film in the IR region. Since solid state devices with metal back electrodes benefit from a "second pass" of light reflected from the back electrode, it is apparent that PEDOT will cause less parasitic absorption losses during this second pass than would spiro-OMeTAD, maximizing the obtainable photocurrent. For devices processed on metal foils, this may be even more important since, in this case, the light is incident from the top, and absorption losses in the visible region by HTM will be of critical importance.

To function effectively as a hole selective contact in photovoltaic devices, PEDOT must be capable of effectively extracting holes from the perovskite absorber layer. We have previously demonstrated that photoluminescence (PL) spectroscopy can be used to monitor charge extraction at the electron and hole selective contacts, where the rate and degree of PL quenching gives a good indication of the charge extraction efficiency.[14] In Figure 1b,c we show the time-resolved and steady-state photoluminescence spectra of perovskite films coated with poly(methyl methacrylate) (PMMA), PEDOT, and spiro-OMeTAD. Both the films coated with spiro-OMeTAD and PEDOT show similar levels of PL quenching with similar decay rates. Therefore, we can infer that the hole-transfer from the perovskite films to PEDOT is similarly good as that to Spiro-OMeTAD.

Once extracted from the perovskite absorber layer, the holes must be effectively transported to the metal cathode to contribute to photocurrent in working solar cells. As a result, the conductivity of the HTM layer is directly related to the series resistance and can limit the fill factor (FF) of the devices, such that substantial conductivities are required for high-performance devices.[13,15] However, there is a limit to the required conductivity until there is no further benefit on reduced series resistance. On the other hand, if the conductivity is too high, there will be a lower shunt resistance in any instance where the HTM makes contact with the n-type collection layer through pinholes in the perovskite layer, and in addition, the recombination rate (or velocity) at the perovskite HTM interface is likely to increase with increasing p-dopant hole-density. We used a four-probe method to measure the conductivity of the different HTM. The average conductivity of spiro-OMeTAD film is $(2.65 \pm 0.51) \times 10^{-4}$S/cm, whereas it is 3 orders of magnitude higher at $(2.69 \pm 0.34) \times 10^{-1}$S/cm for PEDOT. This implies that the series resistance of the devices with PEDOT will be minimized. However, the high conductivity may induce some unfavorable recombination losses.

To fully assess the PEDOT material, we fabricated perovskite solar cells similar to the configuration as reported by Ball et al.[16] In Figure 2a,b we show cartoons illustrating the basic device configuration and their respective energy levels. In Figure 2c,d we show SEM cross-section images of the as fabricated solar cells with PEDOT and spiro-OMeTAD as the HTMs. For the optimized devices in this study, the thickness of the mesoporous Al_2O_3 layer is ∼250 nm, with a perovskite capping layer of ∼300 nm. The thickness of Spiro-OMeTAD is around 350 nm, while the PEDOT hole-transporter layer is about 200 nm. The difference in layer thickness is due to the processability (viscosity, solids content) of the solutions/dispersions.

We recorded the current density−voltage (J−V) characteristics of the as-fabricated solar cells under AM 1.5G simulated sunlight (100 mW cm^{-2}) (Figure 3a). The comparative J−V curves of the best devices highlight the relative photovoltaic performance of the solar cell containing PEDOT and spiro-OMeTAD as HTMs. We first compare the forward bias to short circuit (FB−SC) J−V curves of the two devices and show the device performance parameters in the inset. The small increase in the short-circuit current (J_{sc}) and open-circuit voltage (V_{oc}) is evident for the devices with PEDOT as compared with the Spiro-OMeTAD. The FF, however, shows even more significant improvements with the PEDOT, leading to improved derived power conversion efficiency for the devices incorporating PEDOT (14.5%) as compared to those using Spiro-OMeTAD (12.4%) as HTM. However, we note that

DOI: 10.1021/acs.jpclett.5b00545
J. Phys. Chem. Lett. 2015, 6, 1666−1673

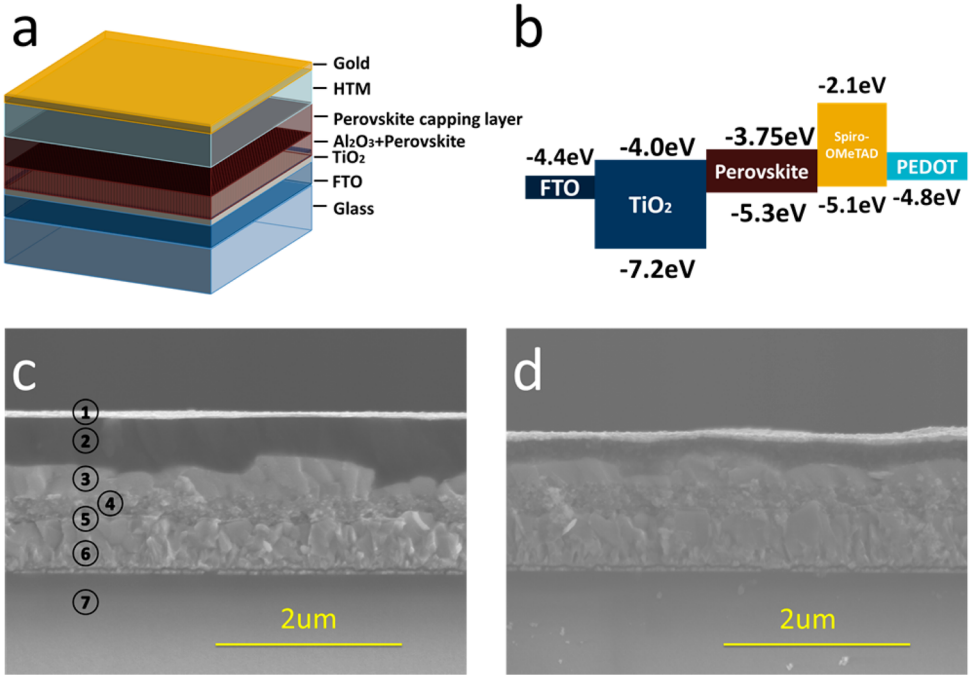

Figure 2. (a) Device schematic. (b) Approximate energy band diagram of the fabricated structure taken from refs 12 and 17. (c,d) Cross-sectional SEM images of photovoltaic device with (c) spiro-OMeTAD and (d) PEDOT as the HTM. The structure from top to bottom are gold, HTM, perovskite, Al_2O_3+perovskite, TiO_2 compact layer, FTO, and glass.

within the experimental spread of average device performance, the solar cell operation is similar to PEDOT and Spiro-OMeTAD (Figure 3c–f), indicating that PEDOT has the ability to perform at least as well as spiro-OMeTAD as the p-type charge collection layer in a perovskite solar cell.

However, there is a non-negligible anomalous hysteresis between the forward bias to short circuit (FB–SC) and the short circuit to forward bias (SC–FB) J–V curves, which is especially pronounced in the solar cells incorporating PEDOT as the hole transporter. From the FB–SC J–V curve of PEDOT solar cell, we can obtain a power-conversion efficiency (PCE) of 14.5%, J_{sc} of 20.2 mA cm^{-2}, V_{oc} of 1.06 V, and FF of 0.68, while, from the SC–FB J–V curve, these numbers go down to 4.9%, 20.2 mA cm^{-2}, 0.62 V, and 0.39, respectively. In the absence of a hole transporter, direct contact of the perovskite with a metal electrode can temporarily function as an effective hole extraction contact. However, the hysteresis is much worse in the case of a metal contact.[18,19] To determine the true steady state stabilized power conversion efficiency of each cell, we show the PCE (%) over time at a fixed voltage close to maximum power point on the FB–SC JV curve, in Figure 3b. After illuminating under 1 sun for 50 s, the PCE (%) of spiro-OMeTAD devices reaches and remains at 9.4%, while the stabilized power output of PEDOT devices can only reach 6.6%. Our studies on anomalous hysteresis thus far indicate that the contact materials can strongly influence hysteresis, and that the forward biasing of the solar cell influences the nature of the contact, to give it a more selective charge collection. If, for instance, hysteresis is pronounced due to an ineffective contact at the electron collection side, then there will be a large buildup of electrons in the perovskite during operation, and less intuitively moreso under short-circuit conditions. If the electron transfer to the TiO_2 is slowed under short-circuit conditions, electronic charge could still flow into the TiO_2 provided the electrons do not recombine with the holes either within the perovskite or at the perovskite hole–transporter heterojunction. Since the PEDOT is much more doped than the spiro-OMeTAD, we would expect a faster recombination at this heterojunction, which would lead to more losses, worse hysteresis, and lower stablised power output, as we observe. Therefore, a key target for future materials development is to reduce the doping level of the PEDOT. We note that this observation appears to be at odds with many reports on "inverted" perovskite solar cells employing PEDOT:PSS and $PC_{61}BM$ as the p- and n-type charge collection layers, respectively, which exhibit low levels of hysteresis.[12,20] However, $PC_{61}BM$ is a very good electron collector when coupled to the $CH_3NH_3PbX_3$, which implies that the electrons will flow out of the perovskite more readily and be less prone to adverse recombination at the perovskite PEDOT interface. An alternative or additional factor may be that PEDOT:PSS is known to stratify upon spin-coating, whereby enrichment of PSS occurs at the surface.[21] This PSS enrichment tunes the work-function, but may also act to reduce the recombination at this interface by assuming the role of an insulating buffer layer.

To further understand the differences we observe here between the devices employing the two hole transport materials, spiro-OMeTAD and PEDOT, we examined the recombination dynamics of the solar cells under conditions where recombination is predominant (i.e., under open-circuit conditions). First, we determined V_{oc} at different values of light intensity (P_{in}) and show the V_{oc} against P_{in} in Figure 4a. According to the standard diode model (assuming no shunt resistances),[22]

$$V_{oc} \propto \frac{2.303nkT}{q} \log_{10} P_{in}$$

where q is the electric charge, k is the Boltzmann's constant, T is the absolute temperature, and n is the ideality diode factor. The derived ideality factors deviated from ideality ($n > 1$) for

DOI: 10.1021/acs.jpclett.5b00545
J. Phys. Chem. Lett. 2015, 6, 1666–1673

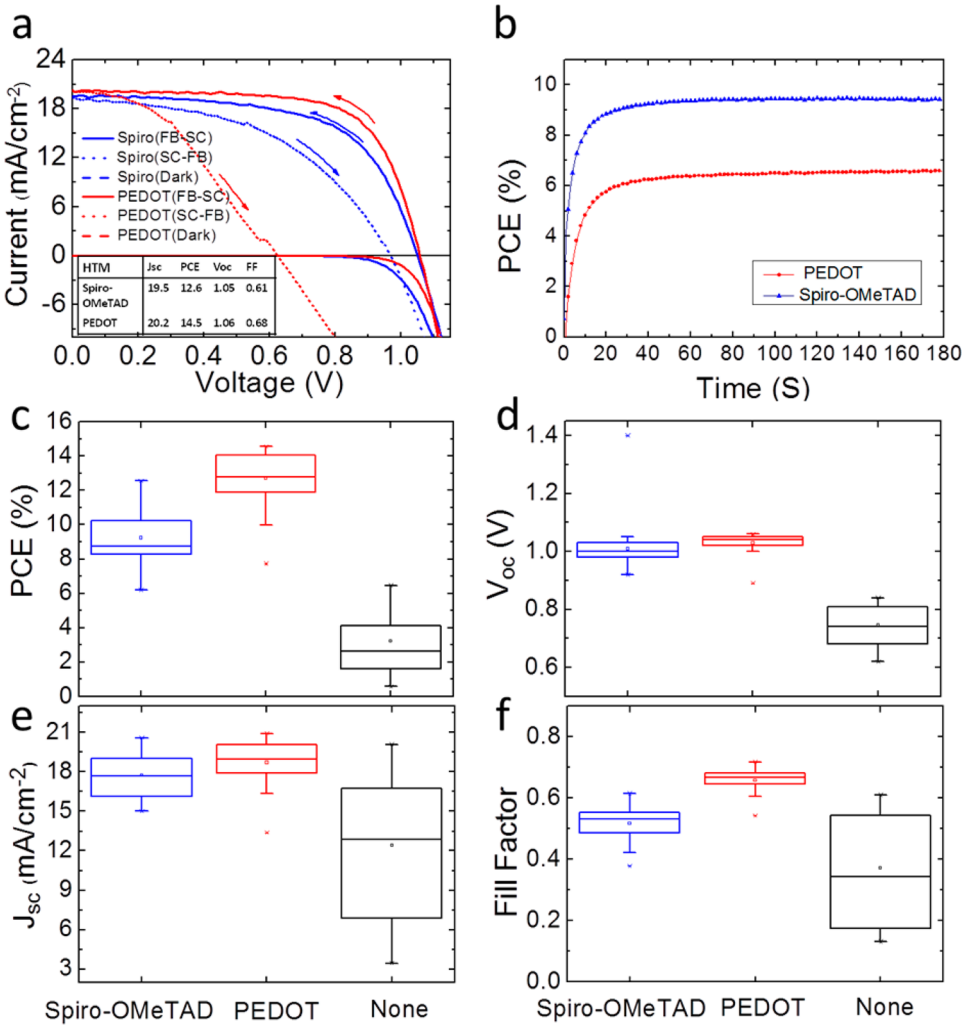

Figure 3. (a) Current voltage curves for best devices of PEDOT (red) and spiro-OMeTAD (blue) configuration. Both forward-bias to short-circuit (FB−SC, solid line) and from short-circuit to forward-bias (SC−FB, dash line) $J-V$ curves are showed. Inset shows the short-circuit current density (J_{sc}, mA cm^{-2}), power-conversion efficiency (PCE, %), open-circuit voltage (V_{oc}, V) and FF for both device architectures determied from the FB−SC JV scans. (b) Power conversion efficiency as a function of time under illumination at a fixed voltage of the maximum power point on the *JV* curve (FB−SC) for best devices of PEDOT (red circles) and spiro-OMeTAD (blue triangles). (c−f) Comparison of PCE, V_{oc}, J_{sc} and FF of solar cells with different configurations (Spiro-OMeTAD, PEDOT and no HTM just Au contact directly onto the perovskite). The data, obtained from an FB−SC scan, are represented as a standard box plot where the box range is defined by 90 percent of all data points fall within the upper and lower whisker. Data points are averaged over 29, 45, and 24 devices for each configuration, respectively.

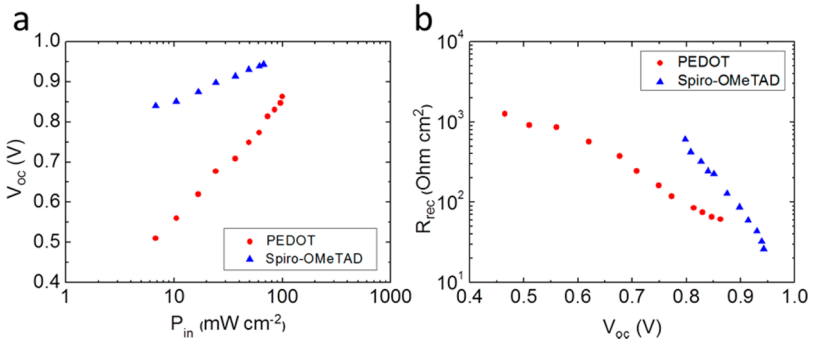

Figure 4. (a) Photovoltage, plotted against the incident light power density and (b) recombination resistance plotted against the V_{oc} for mesostructured solar cells employing spiro-OMeTAD and PEDOT HTMs. The plots were derived by impedance spectroscopy measurements at open-circuit under illumination.

both cells; however, while in the case of spiro, n is ∼2, consistent with literature,[23] the ideality factor of PEDOT containing cell was higher than 5, which is physically unrealistic in a standard diode. We speculate that these unusual high values are caused by severe nonlinear recombination at the interface between PEDOT and the perovskite.[24]

DOI: 10.1021/acs.jpclett.5b00545
J. Phys. Chem. Lett. 2015, 6, 1666−1673

To further justify our findings, we conducted electronic impedance spectroscopy (EIS) under illumination. The spectra exhibit two or three semicircles, in line with previous reports,[25] and therefore we applied the simple model, discussed in the referenced manuscripts here. A full understanding of the origin of the measured capacitances is highly complicated[26,27] and is out of the scope of this work; therefore we have drawn our attention to the recombination resistance, which is the most reliable information derived by EIS fitting.[28] Thus, after fitting, we determine the values for the charge recombination resistance (R_{rec}) and plot R_{rec} against V_{oc} (Figure 4b) according to[29]

$$R_{rec} = R_0 \exp\left[\frac{-\beta q V_{oc}}{kT}\right]$$

where R_0 is the pre-exponential factor, and β is the recombination order.[30] R_{rec} values for spiro-OMeTAD based cells are in very close agreement with results recently reported by Suarez et al., who studied cells of identical structure.[28] Additionally, we found β values to be as high as 0.53 for the spiro-OMeTAD-based cells, in relative agreement with others;[6] by contrast, with PEDOT-based cells we determined β values as low as 0.18. Assuming that the deviation from linearity mostly originates from nonlinear recombination, β should represent the inverse of n;[31] in fact this holds almost entirely true, further justifying our conclusions drawn from V_{oc} versus P_{in} plots (Figure 4a). The clear difference in recombination dynamics between these two cells is consistent with most of the recombination in PEDOT cells arising from the interface between the perovskite and PEDOT, and likely to be due to a trap-mediated process. Our findings are also consistent with the previous work by Guillen et al., who's results indicate that most of the recombination in the current generation of perovskite solar cells occurs at the heterojunction (TiO_2/perovskite or hole transport material/perovskite), and that this type of recombination is likely to take place through surface states.[32]

These results are also consistent with the observation of the importance of the selective contacts in perovskite solar cells in minimizing the level of hysteresis.[19,28,29]

Perovskite films are known to be very sensitive to moisture and temperature, therefore, apart from its main function as a hole collection, the top hole-transporting layer may play a crucial role in terms of acting as a final defense against moisture ingress, and have a strong impact on the thermal resilience of the solar cell, greatly influencing its long-term stability.[33] Different HTMs can protect or damage the perovskite film. Since the PEDOT solution does contain a small amount of water, and PEDOT doped with PSS is known to be hygroscopic due to PSS, we investigate its impact on the perovskite layer here. We spin coated spiro-OMeTAD with and without additives (lithium bis(trifluoromethanesulphonyl)-imide (Li-TFSI) and *tert*-butylpyridine (*t*BP)) and PEDOT on top of perovskite films, and subjected them to thermal stressing (85 °C) up to 72 h in ambient conditions (air with RH ∼ 60%). We recorded photographs and corresponding UV−vis spectra (Figure S1, Supporting Information) at regular intervals (i.e., 0, 6, 20, 36, 48, and 72 h). All samples appear to be stable up to 6 h of heating in air, as they all retain their dark black color. The bare uncoated perovskite film (Figure 5a, row 1) started to degrade within 20 h, noticeable once the film started to turn yellow, indicating the conversion of perovskite to PbI_2.[33] Perovskite films covered with neat spiro-OMeTAD

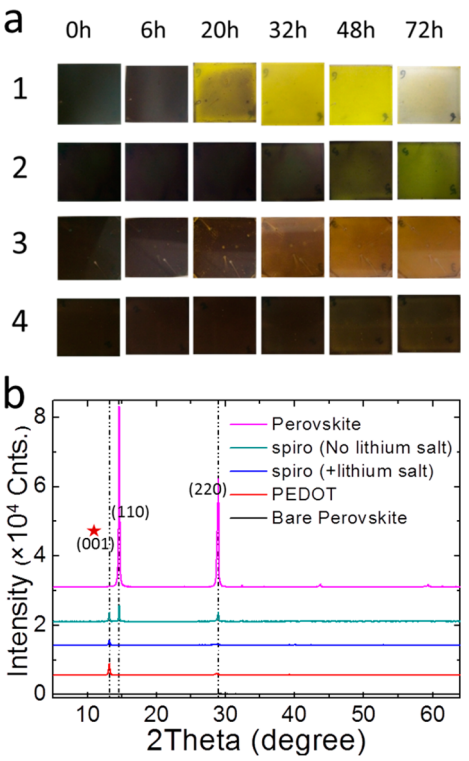

Figure 5. (a) Color change of perovskite film covered with (1) no cover (bare perovskite), (2) PEDOT, (3) spiro-OMeTAD HTM (with Li-TFSI and *t*BP), and (4) neat spiro-OMeTAD. (b) X-ray diffraction pattern of different samples after 72 h of stressing, comparing to a freshly made perovskite sample without aging. The (110) and (220) peaks are from perovskite structure, while the (001) peak (red star) indicates the existence of PbI_2.

(row 4) are the most stable among these samples, as they mostly retain their color even after 72 h of heating. Spiro-OMeTAD with additives (Li-TFSI and *t*BP), however, shows early degradation after 20 h of aging, likely to be due to the hygroscopic nature of the Li-TFSI salt drawing moisture in from the atmosphere. Perovskite film covered with PEDOT on top (row 2) started to change its color after 32 h, which is more stable than the films coated with spiro-OMeTAD with additives containing film but less than those coated with neat spiro-OMeTAD. We show the UV−vis absorption spectra of the respective films at the similar time intervals in the Supporting Information. The photographs match well with the change in absorption spectra where we observe the degradation of perovskite indicated by the loss of perovskite absorption features predominantly at ∼750 nm.

After annealing for 72 h at 85 C in air, these perovskite films coated with Spiro-OMeTAD with and without additives and PEDOT visibly degraded to different extents. To identify the crystal structure after 72 h of annealing in air, we performed X-ray diffraction (XRD) spectroscopy on the films, as we show in Figure 5b. The XRD pattern of freshly made perovskite films shows two main diffraction peaks at 14.63° and 28.98°, indicating the (110) and (220) planes for a tetragonal perovskite structure.[4] After 72 h of aging in air, PEDOT and spiro-OMeTAD doped with Li-TFSI-coated perovskite films show no (110) peak at 14.63°, and we observe instead a strong (001) peak at 13.20°, which can be assigned to PbI_2[34] as an end-product of the perovskite degradation. However, neat spiro-OMeTAD still shows the peaks pertaining to the

DOI: 10.1021/acs.jpclett.5b00545
J. Phys. Chem. Lett. 2015, 6, 1666−1673

perovskite (14.63° and 28.98°) along with the PbI_2 peak at 13.20°[34] The coexistence of peaks pertaining to both perovskite and PbI_2 suggests that the degradation is not complete over 72 h of aging when the perovskite film is coated with the neat spiro-OMeTAD, but notably the films are still partly degraded.

Based on these observations we can infer that these PEDOT films are slightly better than the most efficient spiro-OMeTAD composition containing Li-TFSI and *t*BP at inhibiting thermal degradation of the perovskite films in the presence of moisture. However, they do not protect the perovskite to the same extent as a film of neat spiro-OMeTAD, and by a far lesser extent than carbon nanotubes encapsulated in a PMMA matrix, which we have previously demonstrated.[33] This will be a critical aspect for perovskite solar cells if low levels of encapsulation are required, for instance for flexible applications, or if the moisture sensitivity of the perovskite film cannot be enhanced. However, how important this is for glass-based applications where very effective hematic sealing is possible, is yet to be determined.

In summary, we have demonstrated that PEDOT can be employed as the hole transport layer to fabricate efficient organic−inorganic metal halide perovskite solar cells in the regular configuration where the hole transporter is processed on top of the perovskite film. Devices containing PEDOT perform as well as the commonly used spiro-OMeTAD on measured current voltage curves, but the stabilized power output is lower for the PEDOT cells. Here, we assess the cause for increased hysteresis and reduced stabilized power output and propose that tuning of the doping and conductivity in the PEDOT layer may help improve the stabilized power output in the future. We have also identified that both Li-TFSI-doped spiro-OMeTAD and PEDOT films do not effectively protect the perovskite layer from degradation due to moisture ingress during thermal stressing in ambient conditions, identifying a further area for future development. Despite the current shortcomings, this work identifies the potential for a PEDOT-based organic hole conductor to deliver an extremely inexpensive solution for p-type charge collection from a perovskite solar cell.

METHODS

Device Fabrication. The synthesizing method of $CH_3NH_3PbI_{3-x}Cl_x$ is reported by Lee et al.[4] Fluorine-doped tin oxide (FTO)-coated glass sheets (7 Ω/m^{-1} Hartford) were etched with zinc powder and 2 M HCl for the intended electrode pattern. The substrates were subsequently washed with hellmax, acetone, and ethanol and finally treated under an oxygen plasma etch for 5 min. A solution consists of 0.23 M titanium isopropoxide (Sigma-Aldrich, 99.999%), and 0.013 M HCl solution in ethanol (>99.5%, Sigma-Aldrich) was mixed for depositing TiO_2 compact layer, which was spin-coated at 2000 rpm for 45 s. Substrates were subsequently sintered at 500 °C for 45 min. The mesostructured scaffold was deposited by spin-coating (2000 rpm, 60s) a colloidal dispersion of ∼20 nm Al_2O_3 nanoparticles in isopropanol, followed by drying at 150 °C for 10 min. The substrates were then transferred into a nitrogen filled glovebox. The perovskite layer was deposited in a glovebox under nitrogen atmosphere by spin-coating a dimethylformamide (DMF) solution of methylammonium iodide and $PbCl_2$ (3:1 molar ratio) at 2000 rpm for 45 s, followed by sintering at 100 °C for 90 min. One hundred microliters of iodopentafluorobenzene (Sigma-Aldrich, 99%) was spin-coated on perovskite at 2000 rpm for 45 s before coating the HTM. The deposition of hole transporter layer was also carried out in a glovebox. The spiro-OMeTAD hole transporter layer was deposited by spin-coating an 8.5 vol % solution of Spiro-OMeTAD in chlorobenzene with added 80 mM *t*BP and 25 mM Li-TFSI at 1500 rpm for 50 s. As for the devices with PEDOT as the HTM, the toluene suspension of PEDOT (Clevios NKB 717, Heraeus Deutschland GmbH & Co. KG) was first sonicated for 2 min and then filtered by a 0.45 μm filter. Then the solvent was spin-coated on the substrate when the perovskite had been sintered for 60 min, followed by 30 min sintering at 100 °C. Therefore, the perovskite layer for PEDOT devices had been sintered for 90 min in total, the same as that for the spiro-OMeTAD devices. Finally, the 150 nm Au electrode contact was obtained by evaporation through a shadow mask.

For PEDOT Clevios NKB 717 and Clevios NKB 942, the following parameters were characterized: conductivity by surface resistance measurements in accordance with DIN EN ISO 3915 (conductive polymers) with defined electrode geometry, water content by Karl Fischer titration, and solids content by gravimetric analysis.

Measurement and Characterization. Current−voltage characteristics was measured under simulated AM 1.5 sunlight (ABET Technologies Sun 2000), calibrated to give 100 mW cm^{-2} using an NREL-calibrated KG5-filtered silicon reference cell. The spectral mismatch factor was calculated to be less than 1%. The *J*−*V* curves were recorded with a Keithley 2400. The active area of the solar cells was defined with a metal aperture mask of about 0.0625 cm^2. Scanning electron microscopy (SEM) images were obtained using a Hitachi S-4300.

PL measurement was taken using a time-correlated single photon counting (TCSPC) setup (FluoTime 300, PicoQuant GmbH). Samples were photoexcited using a 510 nm laser head (LDH−P-C-510, PicoQuant GmbH) pulsed at 40 MHz, with a pulse duration of 117 ps and fluence of ∼0.1 nJ/cm^2. Perovskite film was prepared on glass substrate directly as reported by Eperson et al.,[35] with Spiro-OMeTAD and PEDOT as the hole transporter, respectively.

Absorbance spectra were measured with a lambda 1050 UV/vis/NIR spectrometer (PerkinElmer). The samples were prepared by simply spin-coating HTM solvent on glass substrate.

Conductivity measurement was carried out by the four-probe method with a gold probe. Samples were spin-coated hole-transporting layers on glass substrates, followed by evaporating Au electrode pattern through a shadowed mask.

EIS measurements were performed under open-circuit conditions by illuminating the solar cells using a powerful LED array (maximum output power of 306 lm at 700 mA driving current), emitting light at 627 nm. Light intensities were adjusted by controlling the diode's current by a LED driver; the LED was previously calibrated employing a Si reference photodiode. The illuminated area of the solar cells was set at 0.0625 cm^2, using a mask. The spectra were recorded by varying the frequency range from 100 kHz to 40 mHz (amplitude of voltage perturbation: 15 mV RMS) using an electrochemical working station (Autolab PGSTAT302N, Ecochemie) and its built-in frequency response analyzer (FRA2). The recorded spectra were fitted using the NOVA software.

DOI: 10.1021/acs.jpclett.5b00545
J. Phys. Chem. Lett. 2015, 6, 1666−1673

■ ASSOCIATED CONTENT

Supporting Information

UV−vis spectra of perovskite films stressed at regular time intervals. This material is available free of charge via the Internet at http://pubs.acs.org/.

■ AUTHOR INFORMATION

Corresponding Author

*E-mail: h.snaith1@physics.ox.ac.uk.

Notes

The authors declare no competing financial interest.

■ ACKNOWLEDGMENTS

This work was funded in part by the Engineering and Physical Sciences Research Council (EPSRC), the China Scholarship Council (CSC), and the European Union Seventh Framework Programme [FP7/2007-2013] under Grant Agreement No. 604032 of the MESO project. We thank S. Stranks, J. Zhang, W. Zhang, and N. Noel for valuable discussions and experimental and technical assistance.

■ REFERENCES

(1) Chu, S.; Majumdar, A. Opportunities and Challenges for a Sustainable Energy Future. *Nature* **2012**, *488*, 294−303.

(2) Kazmerski, L. *Best Research Cell Efficiencies Chart*; National Renewable Energy Laboratory (NREL): Golden, CO, 2014.

(3) Kojima, A.; Teshima, K.; Shirai, Y.; Miyasaka, T. Organometal Halide Perovskites as Visible-Light Sensitizers for Photovoltaic Cells. *J. Am. Chem. Soc.* **2009**, *131*, 6050−6051.

(4) Lee, M. M.; Teuscher, J.; Miyasaka, T.; Murakami, T. N.; Snaith, H. J. Efficient Hybrid Solar Cells Based on Meso-Superstructured Organometal Halide Perovskites. *Science* **2012**, *338*, 643−647.

(5) Kim, H.-S.; Lee, C.-R.; Im, J.-H.; Lee, K.-B.; Moehl, T.; Marchioro, A.; Moon, S.-J.; Humphry-Baker, R.; Yum, J.-H.; Moser, J. E.; et al. Lead Iodide Perovskite Sensitized All-Solid-State Submicron Thin Film Mesoscopic Solar Cell with Efficiency Exceeding 9%. *Sci. Rep.* **2012**, *2*, 591.

(6) Christians, J. A.; Fung, R. C. M.; Kamat, P. V. An Inorganic Hole Conductor for Organo-Lead Halide Perovskite Solar Cells. Improved Hole Conductivity with Copper Iodide. *J. Am. Chem. Soc.* **2014**, *136*, 758−764.

(7) Ito, S.; Tanaka, S.; Vahlman, H.; Nishino, H.; Manabe, K.; Lund, P. Carbon-Double-Bond-Free Printed Solar Cells from TiO_2 /$CH_3NH_3PbI_3$ /CuSCN/Au: Structural Control and Photoaging Effects. *ChemPhysChem* **2014**, *15*, 1194−1200.

(8) Groenendaal, L.; Jonas, F.; Freitag, D.; Pielartzik, H.; Reynolds, J. R. Poly(3,4-Ethylenedioxythiophene) and Its Derivatives: Past, Present, and Future. *Adv. Mater.* **2000**, *12*, 481−494.

(9) Greczynski, G.; Kugler, T.; Salaneck, W. Characterization of the PEDOT-PSS System by Means of X-ray and Ultraviolet Photoelectron Spectroscopy. *Thin Solid Films* **1999**, *354*, 129−135.

(10) Jönsson, S. K.; Birgerson, J.; Crispin, X.; Greczynski, G.; Osikowicz, W.; Denier van der Gon, A.; Salaneck, W.; Fahlman, M. The Effects of Solvents on the Morphology and Sheet Resistance in Poly(3,4-Ethylenedioxythiophene)−Polystyrenesulfonic Acid (PEDOT−PSS) Films. *Synth. Met.* **2003**, *139*, 1−10.

(11) Kim, Y. H.; Sachse, C.; Machala, M. L.; May, C.; Müller-Meskamp, L.; Leo, K. Highly Conductive PEDOT:PSS Electrode with Optimized Solvent and Thermal Post-Treatment for ITO-Free Organic Solar Cells. *Adv. Funct. Mater.* **2011**, *21*, 1076−1081.

(12) Docampo, P.; Ball, J. M.; Darwich, M.; Eperon, G. E.; Snaith, H. J. Efficient Organometal Trihalide Perovskite Planar-Heterojunction Solar Cells on Flexible Polymer Substrates. *Nat. Commun.* **2013**, *4*, 2761.

(13) Abate, A.; Leijtens, T.; Pathak, S.; Teuscher, J.; Avolio, R.; Errico, M. E.; Kirkpatrik, J.; Ball, J. M.; Docampo, P.; McPherson, I.; et al. Lithium Salts as "Redox Active" P-Type Dopants for Organic Semiconductors and Their Impact in Solid-State Dye-Sensitized Solar Cells. *Phys. Chem. Chem. Phys.* **2013**, *15*, 2572−2579.

(14) Stranks, S. D.; Eperon, G. E.; Grancini, G.; Menelaou, C.; Alcocer, M. J. P.; Leijtens, T.; Herz, L. M.; Petrozza, A.; Snaith, H. J. Electron-Hole Diffusion Lengths Exceeding 1 Micrometer in an Organometal Trihalide Perovskite Absorber. *Science* **2013**, *342*, 341−344.

(15) Leijtens, T.; Lim, J.; Teuscher, J.; Park, T.; Snaith, H. J. Charge Density Dependent Mobility of Organic Hole-Transporters and Mesoporous TiO_2 Determined by Transient Mobility Spectroscopy: Implications to Dye-Sensitized and Organic Solar Cells. *Adv. Mater.* **2013**, *25*, 3227−3233.

(16) Ball, J. M.; Lee, M. M.; Hey, A.; Snaith, H. J. Low-Temperature Processed Meso-Superstructured to Thin-Film Perovskite Solar Cells. *Energy Environ. Sci.* **2013**, *6*, 1739.

(17) Leijtens, T.; Ding, I.-K.; Giovenzana, T.; Bloking, J. T.; McGehee, M. D.; Sellinger, A. Hole Transport Materials with Low Glass Transition Temperatures and High Solubility for Application in Solid-State Dye-Sensitized Solar Cells. *ACS Nano* **2012**, *6*, 1455−1462.

(18) Snaith, H. J.; Abate, A.; Ball, J. M.; Eperon, G. E.; Leijtens, T.; Noel, N. K.; Stranks, S. D.; Wang, J. T.-W.; Wojciechowski, K.; Zhang, W. Anomalous Hysteresis in Perovskite Solar Cells. *J. Phys. Chem. Lett.* **2014**, *5*, 1511−1515.

(19) Zhang, Y.; Liu, M.; Eperon, G. E.; Leijtens, T.; McMeekin, D. P.; Saliba, M.; Zhang, W.; De Bastiani, M.; Petrozza, A.; Herz, L.; et al. Charge Selective Contacts, Mobile Ions and Anomalous Hysteresis in Organic-Inorganic Perovskite Solar Cells. *Mater. Horiz.* **2015**, DOI: 10.1039/C4MH00238E.

(20) Shao, Y.; Xiao, Z.; Bi, C.; Yuan, Y.; Huang, J. Origin and Elimination of Photocurrent Hysteresis by Fullerene Passivation in $CH_3NH_3PbI_3$ Planar Heterojunction Solar Cells. *Nat. Commun.* **2014**, *5*, 5784.

(21) Snaith, H. J.; Kenrick, H.; Chiesa, M.; Friend, R. H. Morphological and Electronic Consequences of Modifications to the Polymer Anode "PEDOT:PSS. *Polymer (Guildford, Engl.)* **2005**, *46*, 2573−2578.

(22) Kirchartz, T.; Deledalle, F.; Tuladhar, P. S.; Durrant, J. R.; Nelson, J. On the Differences between Dark and Light Ideality Factor in Polymer:Fullerene Solar Cells. *J. Phys. Chem. Lett.* **2013**, *4*, 2371−2376.

(23) Agarwal, S.; Seetharaman, M.; Kumawat, N. K.; Subbiah, A. S.; Sarkar, S. K.; Kabra, D.; Namboothiry, M. A.; Nair, P. R. On The Uniqueness of Ideality Factor and Voltage Exponent of Perovskite Based Solar Cells. *J. Phys. Chem. Lett.* **2014**, *5*, 4115−4121.

(24) Gonzalez-Vazquez, J. P.; Oskam, G.; Anta, J. A. Origin of Nonlinear Recombination in Dye-Sensitized Solar Cells: Interplay between Charge Transport and Charge Transfer. *J. Phys. Chem. C* **2012**, *116*, 22687−22697.

(25) Juarez-Perez, E. J.; Wußler, M.; Fabregat-Santiago, F.; Lakus-Wollny, K.; Mankel, E.; Mayer, T.; Jaegermann, W.; Mora-Sero, I. Role of the Selective Contacts in the Performance of Lead Halide Perovskite Solar Cells. *J. Phys. Chem. Lett.* **2014**, *5*, 680−685.

(26) Bisquert, J.; Bertoluzzi, L.; Mora-Sero, I.; Garcia-Belmonte, G. Theory of Impedance and Capacitance Spectroscopy of Solar Cells with Dielectric Relaxation, Drift-Diffusion Transport, and Recombination. *J. Phys. Chem. C* **2014**, *118*, 18983−18991.

(27) Pockett, A.; Eperon, G. E.; Peltola, T.; Snaith, H. J.; Walker, A. B.; Peter, L. M.; Cameron, P. J. Characterization of Planar Lead Halide Perovskite Solar Cells by Impedance Spectroscopy, Open Circuit Photovoltage Decay and Intensity-Modulated Photovoltage/Photocurrent Spectroscopy. *J. Phys. Chem. C* **2015**, *119*, 3456−3465.

(28) Suarez, B.; Gonzalez-Pedro, V.; Ripolles, T. S.; Sanchez, R. S.; Otero, L.; Mora-Sero, I. Recombination Study of Combined Halides (Cl, Br, I) Perovskite Solar Cells. *J. Phys. Chem. Lett.* **2014**, *5*, 1628−1635.

(29) Fabregat-Santiago, F.; Garcia-Belmonte, G.; Mora-Seró, I.; Bisquert, J. Characterization of Nanostructured Hybrid and Organic

DOI: 10.1021/acs.jpclett.5b00545
J. Phys. Chem. Lett. 2015, 6, 1666−1673

Solar Cells by Impedance Spectroscopy. *Phys. Chem. Chem. Phys.* **2011**, *13*, 9083−9118.
(30) Bisquert, J.; Mora-Seró, I. Simulation of Steady-State Characteristics of Dye-Sensitized Solar Cells and the Interpretation of the Diffusion Length. *J. Phys. Chem. Lett.* **2010**, *1*, 450−456.
(31) Barnes, P. R. F.; Miettunen, K.; Li, X.; Anderson, A. Y.; Bessho, T.; Gratzel, M.; O'Regan, B. C. Interpretation of Optoelectronic Transient and Charge Extraction Measurements in Dye-Sensitized Solar Cells. *Adv. Mater.* **2013**, *25*, 1881−1922.
(32) Gonzalez-Vazquez, J. P.; Oskam, G.; Anta, J. A. Origin of Nonlinear Recombination in Dye-Sensitized Solar Cells: Interplay between Charge Transport and Charge Transfer. *J. Phys. Chem. C* **2012**, *116*, 22687−22697.
(33) Habisreutinger, S. N.; Leijtens, T.; Eperon, G. E.; Stranks, S. D.; Nicholas, R. J.; Snaith, H. J. Carbon Nanotube/Polymer Composite as a Highly Stable Charge Collection Layer in Perovskite Solar Cells. *Nano Lett.* **2014**, *14*, 5561−5568.
(34) Liu, M.; Johnston, M. B.; Snaith, H. J. Efficient Planar Heterojunction Perovskite Solar Cells by Vapour Deposition. *Nature* **2013**, *501*, 395−398.
(35) Eperon, G. E.; Burlakov, V. M.; Docampo, P.; Goriely, A.; Snaith, H. J. Morphological Control for High Performance, Solution-Processed Planar Heterojunction Perovskite Solar Cells. *Adv. Funct. Mater.* **2014**, *24*, 151−157.

DOI: 10.1021/acs.jpclett.5b00545
J. Phys. Chem. Lett. 2015, 6, 1666−1673